Enhancement of Mixing and Reaction in High-Speed Combustor Flowfields

J. Philip Drummond
NASA Langley Research Center
Hampton, Virginia

International Colloquium on Advanced Computation and
Analysis of Combustion
May 12-15, 1997
Moscow, RUSSIA

Advanced Computation & Analysis of Combustion: 1–14

ENHANCEMENT OF MIXING AND REACTION IN HIGH-SPEED COMBUSTOR FLOWFIELDS

J. Philip Drummond

NASA Langley Research Center, Hampton, Virginia 23681

1 Introduction

Research has been underway for a number of years, both in the United States and abroad, to develop advanced aerospace propulsion systems for use late in this century and beyond. One program is now underway at the NASA Langley Research Center to develop a hydrogen-fueled supersonic combustion ramjet (scramjet) that is capable of propelling a vehicle at hypersonic speeds in the atmosphere. A part of that research has been directed toward the optimization of the scramjet combustor and, in particular, the efficiency of fuel–air mixing and reaction taking place in the engine. In the high-speed vehicle configurations currently being considered, achieving a high combustor efficiency becomes particularly difficult. With increasing combustor Mach number, the degree of fuel–air mixing that can be achieved through natural convective and diffusive processes is reduced leading to an overall decrease in combustion efficiency and thrust.

Compressible shear layers and jets provide a good model for studying the physical processes occurring in high speed mixing and combustion in a scramjet. Mixing layers are characterized by large scale eddies that form due to the high shear that is present between the fuel and the air streams [1]. These eddies entrain the fuel and air into the mixing region between the fluids leading to increased surface area and locally steep concentration gradients. Molecular diffusion then occurs across the strained interfaces. In an early study of high-speed mixing, Brown and Roshko [1] show that the spreading rate of a supersonic mixing layer decreases with increasing Mach number, exhibiting a factor of three decrease in spread rate as compared with an incompressible mixing layer with the same density ratio. They conclude that the reduced spread rate is primarily due to compressibility. Papamoschou and Roshko [2, 3] also observe that the spreading rate of compressible mixing layers is significantly reduced over that of incompressible layers. To characterize the structure of the flow quantitatively, they define a convective Mach number [4]. The reduction in mixing layer spreading rate is shown in these experiments to correlate well with increasing convective Mach number.

Within the past decade, compressible mixing layers have been the subject of numerous investigations via stability analysis [5]–[8], numerical simulations [9]–[17] and laboratory experiments [18]–[21]; see [22]–[24] for reviews. These investigations

generally indicate that increased compressibility reorganizes the turbulence field and modifies the development of turbulent structures. The resulting suppressed transverse Reynolds normal stresses seem to result in reduced momentum transport. In addition, the primary Reynolds stresses responsible for mixing layer growth rate are also reduced. All of these effects combine to reduce the growth rate of the mixing layer and the overall level of mixing that is achieved.

Because of these difficulties, attention has now turned to the development of techniques for enhancing the rate of fuel–air mixing in the combustor. Several techniques have been developed for enhancing the mixing rates in supersonic mixing layers and jets. Guirguis *et al.* [25] show that the spreading rate of a confined mixing layer can be improved if the pressure of the two streams is different. Encouraged by this result, Guirguis [26] employed a bluff body at the base of the splitter plate separating the two streams. It is shown that the body produces an instability further upstream in the layer and results in a more rapid rate of spread. Kumar *et al.* [27] discuss a number of mixing problems that may exist in scramjet combustors. Several techniques for enhancing turbulence and mixing in combustor flow fields are suggested, and one enhancement technique that employs an oscillating shock is studied numerically. Drummond and Mukunda [28] have studied fuel–air mixing and reaction in a supersonic mixing layer and have applied several techniques for enhancing mixing and combustion in the layer. They show that when the mixing layer, with its large gradients in velocity and species, is processed through a shock with strong curvature, vorticity is produced. The vorticity then interacts with the layer and results in a significant increase in the degree of mixing and reaction. Drummond *et al.* [29, 10] continued this investigation further by studying fuel–air mixing in a supersonic combustor. They describe a technique using swept-wedge fuel injectors [30] to enhance the mixing processes and overall combustion efficiency in the flow. The swept-wedge injectors introduce streamwise vorticity in the inlet air passing over them, and that air then entrains fuel being injected from the base of the strut. Fuel–air mixing efficiency is shown to be significantly improved by the fuel-jet–air interaction.

Marble *et al.* [31, 32] employ a planar oblique shock to enhance the mixing between a co-flowing circular helium or hydrogen jet and air. They show that when the jet is processed by the oblique shock, a strong vorticity component is induced at the interface between the low density jet and the relatively high density airstream by the pressure gradient of the shock. Vorticity is generated when the density and pressure gradients are not aligned. The induced vorticity in the fuel jet provides a significant degree of mixing enhancement.

This paper describes a numerical study of candidate mixing strategies to enhance fuel–air mixing and reaction in scramjet engines. The first approach considered is a wedge shaped fuel injector that enhances mixing by introducing streamwise vorticity produced by the body. The second approach involves the production of

streamwise vorticity through the proper interaction of pressure and density fields in the combustor flowfield.

2 Theory

The flow field considered in this study is described by the three-dimensional (3D) Navier–Stokes, energy, and species continuity equations governing multiple species fluid undergoing chemical reaction [9, 33, 34]. The finite-rate chemical reaction of gaseous hydrogen and air is modeled with a seven-species, seven-reaction model. The coefficients governing the diffusion of momentum, energy, and mass are determined from models based on kinetic theory [9]. Sutherland's law is employed to compute the individual species viscosity; the mixture viscosity is evaluated by the Wilke's law. An alternate form of Sutherland's law is also used to compute the individual species thermal conductivity. The mixture thermal conductivity is then determined by the Wassilewa's formula. The Chapman and Cowling law is used to determine the binary diffusion coefficients which describe the diffusion of each species into the remaining species. Knowing the diffusion coefficients, the diffusion velocities of each species are determined by solving the multicomponent diffusion equation [9].

Once the thermodynamic properties, chemical production rates, and diffusion coefficients have been computed, the governing equations are solved with the 3D SPARK computer code using Carpenter's convective fourth-order symmetric predictor-corrector compact algorithm [33]. The algorithm is constructed on a compact three by three stencil which provides high-order accuracy while allowing boundary conditions to be specified to fourth-order accuracy in a straightforward manner. Details of the algorithm are given by Carpenter [33].

3 Results

3.1 Mixing Enhancement Using Swept Wedges

A number of approaches have been suggested for enhancing the mixing of high-speed fuel–air flows. Several of these approaches are discussed in the Introduction. A particularly attractive option has been suggested by Northam *et al.* [30] in their experimental study of wall mounted parallel injector ramps used to enhance the relatively slow mixing of fuel and air normally associated with parallel fuel injection. Parallel injection may be useful at high speeds to extract energy from hydrogen that has been used to cool the engine and the airframe of a hypersonic cruise vehicle. The ramp injector configurations are intended to induce vortical flow and local recirculation regions similar to the rearward-facing step that has been used for flame holding in reacting supersonic flow.

It is instructive to study some aspects of these experiments here. Two ramp configurations are considered in the experiment of Northam *et al.* [30] as shown in Fig. 1.

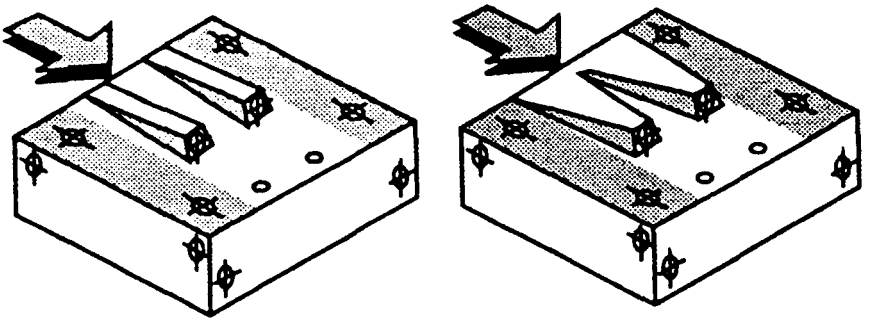

a) b)

Figure 1. Unswept (a) and Swept (b) ramp fuel–injector configurations

In both configurations, hydrogen gas is injected at Mach 1.7 from conical nozzles in the base of the two ramps which are inclined at 10.3 degrees to the combustor wall. The injector diameters are 0.762 cm. The sidewalls of the unswept ramps are aligned with Mach 2 streamwise airflow from a combustion facility, whereas the swept ramps are swept at an angle of 80 degrees. Each ramp is 7 cm long and ends in a nearly square base, 1.52 cm on a side.

Both ramp designs are chosen to induce vorticity to enhance mixing and base flow recirculation to provide flame holding. The swept ramp injector, because of its delta shape, is intended to induce higher levels of vorticity and, therefore, higher levels of mixing. Hydrogen injection occurs at a streamwise velocity of 1 747 m/s, a transverse velocity of 308 m/s, and a static temperature and pressure of 187 K and 325 200 Pa, respectively. The facility air crosses the leading edge of the wedges at a streamwise velocity of 1 300 m/s, a static temperature of 1 023 K, and a static pressure of 102 000 Pa. The air is vitiated following heating by a burner with oxygen, nitrogen, and water mass fractions of 0.2551, 0.5533, and 0.1818, respectively. The overall fuel–air equivalence ratio is 0.6. Both the unswept and swept parallel injector ramps are studied computationally. Only fuel–air mixing is considered. The facility test section surrounding the ramps and considered in the computation is 13.97 cm long and 3.86 cm high. Symmetry planes are chosen to pass transversely through each fuel injector to define the spanwise computational boundaries.

Results from the computational study for both the unswept and swept injector ramps are shown in Figs. 2–5. Figures 2 and 3 show the cross-stream velocity vectors for the unswept and swept cases at two downstream planes (x = 6.6 and 13.2 cm) oriented perpendicular to the test section walls. Part (a) of the figures displays the unswept ramp results and part (b) shows the swept ramp results. The planar cut extends from the lower to the upper wall of the test section, and it slices through the center of the right fuel jet. The left boundary is located halfway between

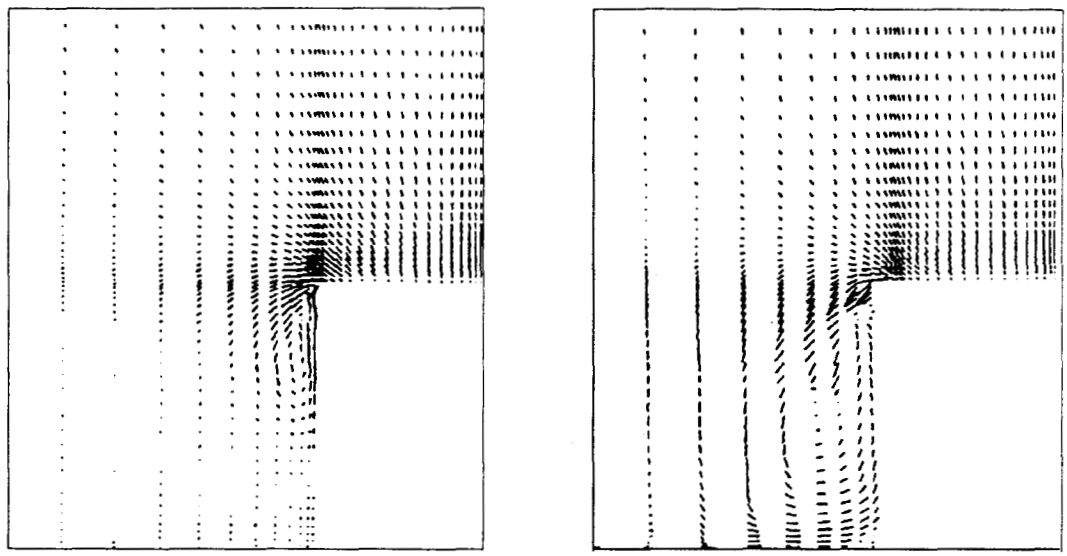

Figure 2. Cross-stream velocity vectors for (*a*) unswept, and (*b*) swept, ramp at $x = 6.60$ cm

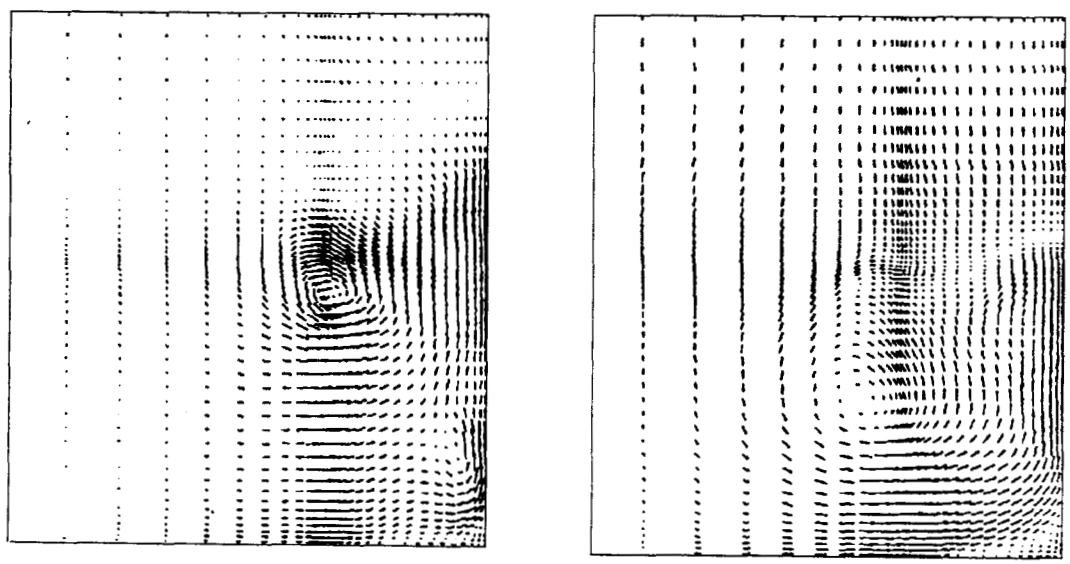

Figure 3. Cross-stream velocity vectors for (*a*) unswept, and (*b*) swept, ramp at $x = 13.2$ cm

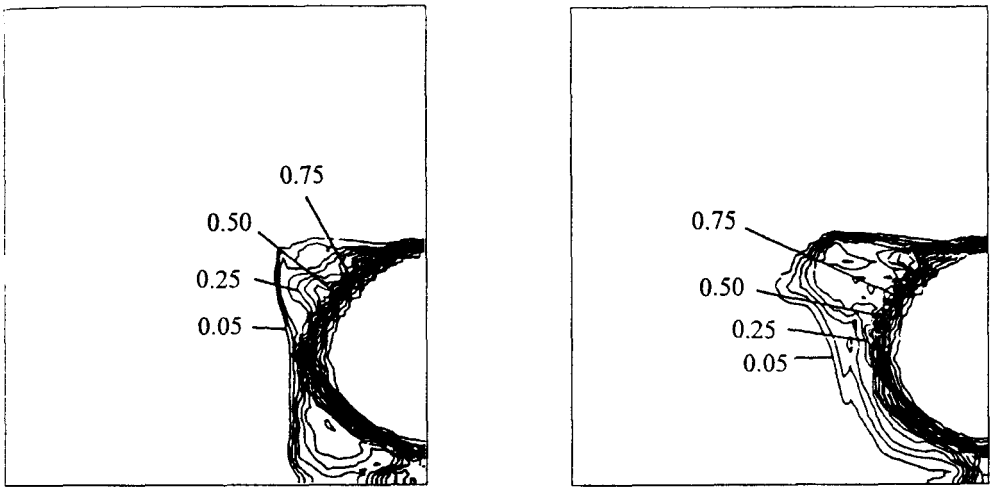

Figure 4. Cross-stream hydrogen mass fraction contours for (*a*) unswept, and (*b*) swept, ramp at $x = 7.30$ cm

the two ramps. At the $x = 6.6$ cm station, which lies just ahead of the end of the ramps, a streamwise vortex has formed at the edge of each ramp. The vortex formed by the swept ramp is considerably larger, however, and it persists well into the flow above the ramp and to the ramp centerline. At the $x = 13.2$ cm station, located 6.2 cm beyond the end of the ramps, the swept ramp vortex has significantly grown and has moved well toward the jet centerline. The swept ramp vortex has now interacted with the hydrogen fuel jet, enhancing its penetration into the airstream. There is pronounced fuel–air mixing enhancement as the vortex spreads across the test section, convecting hydrogen fuel into the airstream. Some enhancement is also provided by the unswept ramp, but it is not nearly as pronounced as that provided by the swept ramp.

The transport of hydrogen fuel into the airstream can be observed more clearly by studying the location of hydrogen mass fraction contours in two test section cross planes, plotted with increasing streamwise distance. Figures 4 and 5 show the hydrogen mass fraction contours at two successive downstream planes ($x = 7.3$ and 13.2 cm), again oriented perpendicular to the test section walls. As before, part (*a*) of the figures displays the unswept ramp results, and part (*b*) displays the swept ramp results. The results in Fig. 4 occur 0.3 cm downstream of the end of the ramp. With the swept ramp, the larger streamwise vortex has already begun to sweep the hydrogen fuel across into the airstream and away from the lower wall. The smaller streamwise vortex of the unswept ramp also begins to transport hydrogen away from the jet, but not nearly as much as does the swept ramp. As a result, more hydrogen is transported toward the lower wall boundary layer in the unswept case. These trends

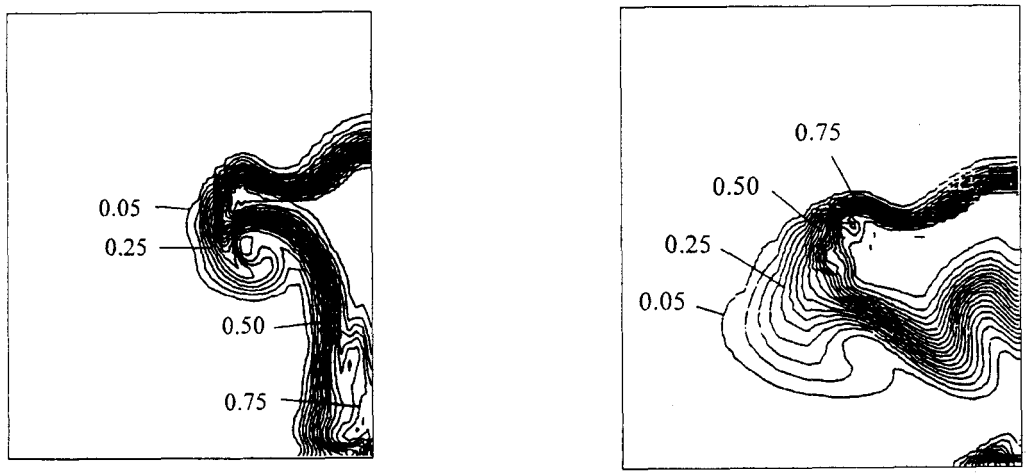

Figure 5. Cross-stream hydrogen mass fraction contours for (*a*) unswept, and (*b*) swept, ramp at $x = 13.2$ cm

continue downstream. At $x = 13.2$ cm, as shown in Fig. 5, the swept ramp enhancer has lifted the fuel jet almost completely off the lower wall. Significant amounts of hydrogen have also been carried across the test section. On the other hand, the unswept ramp enhancer still allows a large amount of hydrogen to be transported along the lower wall, and the spanwise transport is not nearly as great. The spanwise spread of the fuel jet enhanced by the swept ramp is 46 percent greater than the spanwise spread due to the unswept ramp. In addition, the swept enhancer has resulted in the fuel jet being transported completely off the lower wall. Finally, an eddy of hydrogen has broken completely away from the primary hydrogen jet, increasing the fuel–air interfacial area even further. Clearly then, the swept ramp enhancer significantly increases the overall spread and mixing of the hydrogen fuel jets.

3.2 Mixing Enhancement Using Shocks

Following the analysis of swept wedge injectors, a study of the parallel fuel jet configuration described in the Introduction is conducted. As noted before, fuel injected parallel to inlet air entering a combustor is normally assumed to mix relatively slowly with that air. Therefore, to employ parallel injection, it is quite important to enhance mixing of parallel fuel jets and air to the greatest extent possible.

The configuration used for the study of enhanced mixing of parallel fuel jets and air is shown in Fig. 6. It consists of a parallelepiped 6 cm long with a square cross-section 2 cm on a side. A circular hydrogen jet with a 2 mm diameter is injected into the domain from the left face. The hydrogen gas is introduced with a streamwise exponential velocity profile with a peak centerline value of 2 883 m/s, a temperature

of 1 000 K, and a pressure of 101 325 Pa (1 atm.), resulting in a peak hydrogen Mach number of 1.2. Air, co-flowing with the hydrogen, is also introduced from the left face at a velocity of 1 270 m/s, a temperature of 1 000 K, and a pressure of 101 325 Pa, resulting in an air Mach number of 2. An oblique shock is introduced across the flow from the lower wall, by a 10 degree wedge also shown in Fig. 6. In the computations, the shock is produced by specifying the appropriate jump conditions for a 10 degree turning angle along the lower boundary where the shock enters the domain.

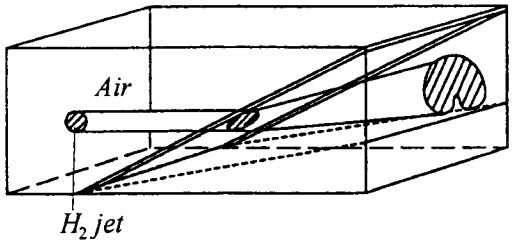

Figure 6. Schematic of shocked, parallel hydrogen fuel jet in air

To establish a baseline for mixing and chemical reaction, calculations are first carried out without the shock. These calculations are conducted for 4 ms in time until a pseudo-steady state is reached following 85 computational sweeps of the flow field. Results for this computation are presented in Figs. 7–14. Figure 7 shows the streamwise development of the hydrogen jet along its centerline in the x–z plane. Values of the hydrogen mass fraction, shown as contours in the figure, are defined in the legend. The hydrogen jet develops very slowly with only a small degree of mixing.

The cross-stream hydrogen mass fraction distribution at the 6 cm station is shown in Fig. 8. It is also clear from this figure that very little mixing of the hydrogen and air has occurred at the end of the domain, with peak values of hydrogen mass fraction as high as 0.56 still persisting in the flow. Figures 9 and 10 show the water mass fraction resulting from chemical reaction in the x–z and y–z planes, respectively. Due to poor fuel–air mixing, reaction occurs only on the edge of the hydrogen jet, and peak values of water mass fraction of only 0.008 are achieved in the outflow cross-plane at $x = 6$ cm. Combustion efficiency for this case rises to only 0.4 percent at the 6 cm station. Combustion efficiency is defined as the ratio of hydrogen in water to the total hydrogen, integrated over each cross-plane. Therefore, credit in efficiency is taken only for exothermically produced final product water, and not for the remaining product species.

To enhance the degree of mixing and combustion of the hydrogen jet and air, the flow is then processed through the 10 degree shock. It was earlier noted that the shock causes the hydrogen jet to split into a vortex pair and spread quickly downstream. The vortices convect hydrogen away from the jet centerline in a spanwise and transverse direction, entraining and mixing the hydrogen with the surrounding airstream.

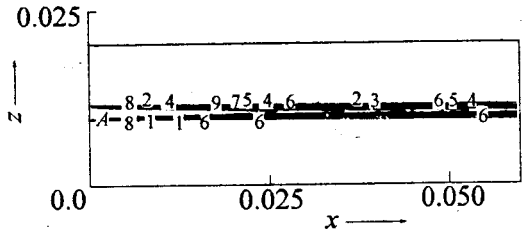

Figure 7. Hydrogen mass fraction of reacting, unshocked jet in x–z plane at $y = 1$ cm. H_2 level: *1* — 0.602, *2* — 0.160, *3* — 0.257, *4* — 0.354, *5* — 0.451, *6* — 0.549, *7* — 0.646, *8* — 0.743, *9* — 0.840, *A* — 0.938

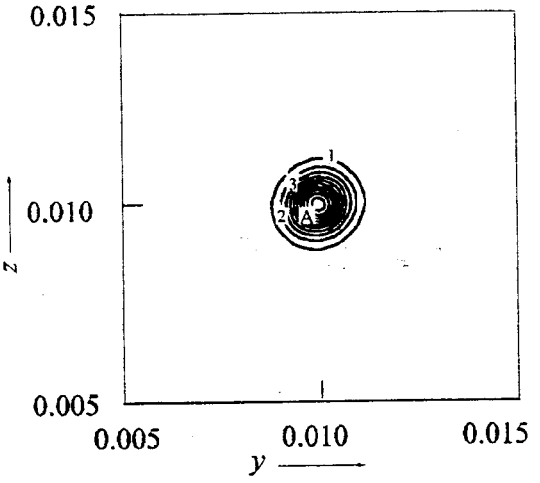

Figure 8. Hydrogen mass fraction of reacting, unshocked jet in y–z plane at $x = 6$ cm. H_2 level: *1* — 0.037, *2* — 0.095, *3* — 0.153, *4* — 0.210, *5* — 0.268, *6* — 0.326, *7* — 0.384, *8* — 0.441, *9* — 0.499, *A* — 0.557

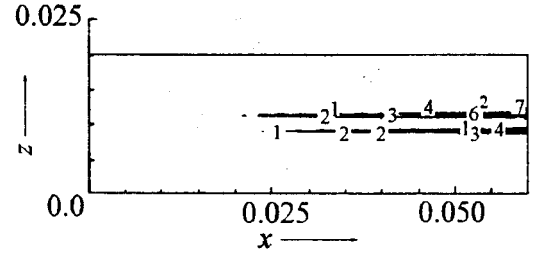

Figure 9. Water mass fraction of reacting, unshocked jet in x–z plane at $y = 1$ cm. H_2O level: *1* — 0.0005, *2* — 0.0009, *3* — 0.0014, *4* — 0.0018, *5* — 0.0023, *6* — 0.0027, *7* — 0.0032, *8* — 0.0037, *9* — 0.0041, *A* — 0.0046

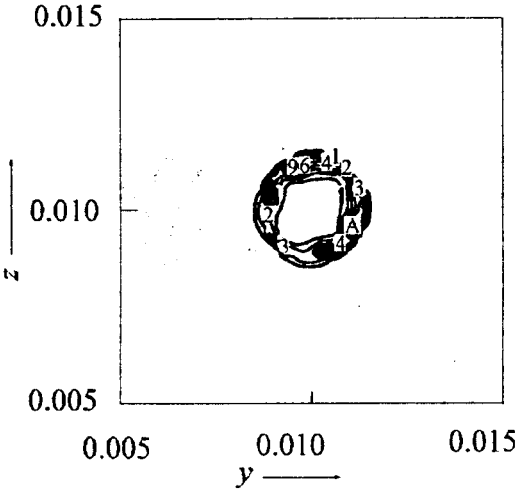

Figure 10. Water mass fraction of reacting, unshocked jet in y–z plane at $x = 6$ cm. H_2O level: *1* — 0.0008, *2* — 0.0017, *3* — 0.0025, *4* — 0.0034, *5* — 0.0042, *6* — 0.0050, *7* — 0.0059, *8* — 0.0067, *9* — 0.0075, *A* — 0.0084

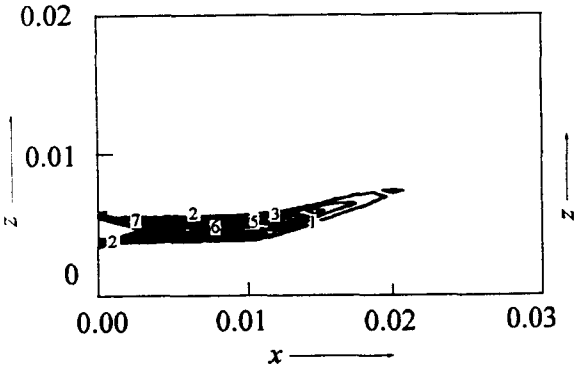

Figure 11. Hydrogen mass fraction of reacting, shocked jet in x–z plane at $y = 1$ cm. H_2 level: *1* — 0.091, *2* — 0.182, *3* — 0.273, *4* — 0.364, *5* — 0.455, *6* — 0.545, *7* — 0.636, *8* — 0.727, *9* — 0.818, *A* — 0.909

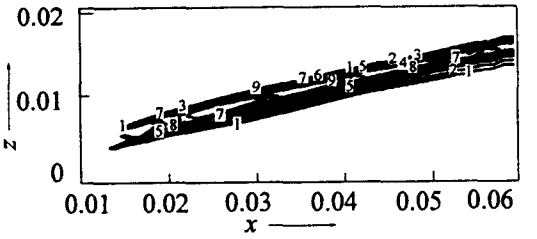

Figure 12. Water mass fraction of reacting, unshocked jet in x–z plane at $y = 1$ cm. H_2O level: *1* — 0.050, *2* — 0.072, *3* — 0.094, *4* — 0.117, *5* — 0.139, *6* — 0.16, *7* — 0.183, *8* — 0.206, *9* — 0.228, *A* — 0.250

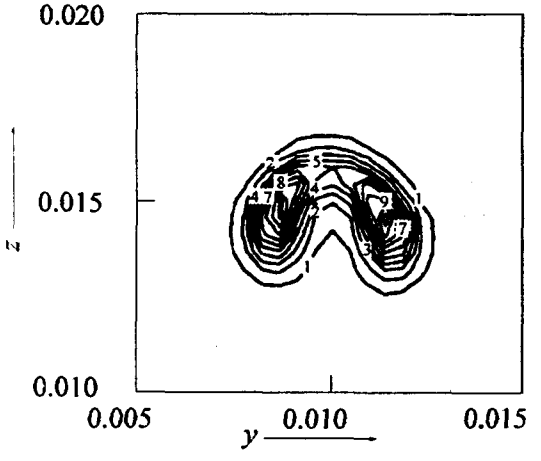

Figure 13. Hydrogen mass fraction of reacting, shocked jet in y–z plane at $x = 6$ cm. H_2 level: *1* — 0.0008, *2* — 0.0021, *3* — 0.0033, *4* — 0.0046, *5* — 0.0059, *6* — 0.0071, *7* — 0.0084, *8* — 0.0097, *9* — 0.0109, *A* — 0.0122

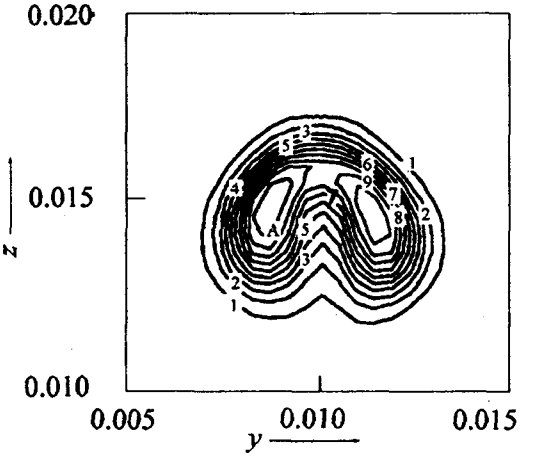

Figure 14. Water mass fraction of reacting, shocked jet in y–z plane at $x = 6$ cm. H_2O level: *1* — 0.0205, *2* — 0.0410, *3* — 0.0614, *4* — 0.0819, *5* — 0.1024, *6* — 0.1229, *7* — 0.1434, *8* — 0.1639, *9* — 0.1843, *A* — 0.2048

Reacting results for the shocked jet are given in Figs. 11–14. Figure 11 shows the streamwise development of the hydrogen jet along its centerline in the x–z plane. The jet passes through the shock at $x = 1.1$ cm and flows downstream at an angle of 10 degrees to the original horizontal path. Due to jet mixing and initial chemical reaction, no hydrogen mass fraction contour greater than 0.09 exists beyond the 2 cm station. The water mass fraction distribution resulting from reaction is shown in Fig. 12. Water production begins a short distance downstream of the shock. Peak water production at each station occurs downstream along the stoichiometric line roughly located 75 percent across the water profile. This location is coincident with the lower hydrogen concentration lying between and above the stable hydrogen vortex pair. However, water production is still significant above and below this line as indicated in Fig. 12.

Due to the interaction of gradients of the pressure and density at the shock–jet–air interface, two streamwise vortices have formed in the hydrogen jet, with the left vortex containing positive and the right vortex containing negative components of vorticity when viewed from the outflow of the domain. This vortex structure distorts the initial circular cross-section of the hydrogen jet, entraining fuel and air and enhancing mixing. The jet distortion can be seen in Fig. 13 which shows the hydrogen species mass fractions at the $x = 6$ cm station. Hydrogen is concentrated toward the interior of each vortex with peak values of around 0.012. Hydrogen is stretched away from the upper portion of the jet, however, and the mass fraction is most greatly reduced in that region. This region of reduced concentration favors the highest initial degree of combustion since the fuel–air ratio is nearest to stoichiometric conditions.

Figure 14 shows the resulting water mass fraction distribution in the y–z plane at the $x = 6$ cm station. Combustion begins in the stoichiometric region at the top of the vortices and along the outer edge of the remainder of the vortices. At $x = 6$ cm, the flame has propagated into the interior of the vortex structure such that significant reaction is occurring near the center of each vortex. The peak water mass fraction of 0.2 occurs at this location. There is also a significant temperature rise near the top and near the center of the vortices due to reaction. It is quite interesting to compare the resulting combustion efficiency for the shocked reacting jet case with the unshocked reacting jet case. Recall that in the unshocked case, the combustion efficiency at $x = 6$ cm is only 0.4 percent whereas in the shocked case, a combustion efficiency of 72 percent is achieved.

4 Concluding Remarks

In high-speed airbreathing propulsion systems, the extent of fuel–air mixing is significantly reduced with increasing Mach number. Direct numerical simulations of reacting mixing layer flows, as described in the references, indicate that there is a reduction in turbulence levels due to an increase in either Mach number or heat release. To counter the effects of suppressed mixing and reaction, two mixing en-

hancement techniques have been developed. The first one involves the use of swept wedges placed in the airstream to introduce longitudinal vorticity leading to large scale mixing enhancement. The second technique utilizes the interaction of a shock with the large density gradient existing between a hydrogen fuel jet and the surrounding airstream to introduce streamwise vorticity and mixing. Both of these approaches have proven effective in providing mixing enhancement mechanisms in nonpremixed high-speed reacting flows.

References

[1] Brown, G.L. and Roshko, A., "On Density Effects and Large Structure in Turbulent Mixing Layers", *J. Fluid Mech.*, **64**, 775–816, 1974.

[2] Papamoschou, D. and Roshko, A., Observations of Supersonic Free Shear Layers, AIAA Paper No. 86–0162, 1986.

[3] Papamoschou, D. and Roshko, A., "The Compressible Turbulent Shear Layer: An Experimental Study", *J. Fluid Mech.*, **197**, 453–477, 1988.

[4] Bogdanoff, D.W., "Compressibility Effects in Turbulent Shear Layers", *AIAA Journal*, **21**, 926–927, 1983.

[5] Jackson, T.L. and Grosch, C.E., "Inviscid Spatial Stability of a Compressible Mixing Layer", *J. Fluid Mech.*, **208**, 609–637, 1989.

[6] Jackson, T.L. and Grosch, C.E., "Inviscid Spatial Stability of a Compressible Mixing Layer. Part 2. The Flame Sheet Model", *J. Fluid Mech.*, **217**, 391–420, 1990.

[7] Ragab, S.A. and Wu, J.L., "Linear Instabilities in Two-Dimensional Compressible Mixing Layers", *Phys. Fluids A*, **1**, 957–966, 1989.

[8] Jackson, T.L., "A Review of Spatial Stability Analysis of Compressible Reacting Mixing Layers", *Major Research Topics in Combustion*, (Eds. M.Y. Hussaini, A. Kumar, and R.G. Voigt), Springer-Verlag, New York, NY, 131–161, 1992.

[9] Drummond, J.P., "Two-Dimensional Numerical Simulation of a Supersonic, Chemically Reacting Mixing Layer", *NASA TM 4055*, 1988.

[10] Drummond, J.P., Carpenter, M.H., and Riggins, D.W., "Mixing and Mixing Enhancement in Supersonic Reacting Flow Fields", *High Speed Propulsion Systems, AIAA Progress Series*, **137**, (Eds. S.N.B. Murthy and E.T. Curran), American Institute of Aeronautics and Astronautics, Washington, D.C., ch. 7, 383–455, 1991.

[11] Soetrisno, M., Eberhardt, D.S., Riley, J.J., and McMurtry, P.A., A Study of Inviscid, Supersonic Mixing Layers Using a Second-Order TVD Scheme, AIAA Paper No. 88–3676–CP, 1988.

[12] Lele, S.K., Direct Numerical Simulation of Compressible Free Shear Flows, AIAA Paper No. 89–0374, 1989.

[13] Sandham, N.D. and Reynolds, W.C., A Numerical Investigation of the Compressible Mixing Layer, Stanford University, Department of Mechanical Engineering, Thermosciences Division, Stanford, CA., Report No. TF–45, 1989.

[14] Givi, P., Madnia, C.K., Steinberger, C.J., Carpenter, M.H., and Drummond, J.P., "Effects of Compressibility and Heat Release in a High Speed Reacting Mixing Layer", *Combust. Sci. Tech.*, **78**, 33–68, 1991.

[15] Grinstein, F.F. and Kailasanath, K., Chemical Energy Release, Spanwise Excitation, and Dynamics of Transitional, Reactive, Free Shear Flows, AIAA Paper No. 91–0247, 1991.

[16] Mukunda, H.S., Sekar, B., Carpenter, M.H., Drummond, J.P., and Kumar, A., "Direct Simulation of High–Speed Mixing Layers", *NASA TP 3186*, 1992.

[17] Planche, O.H. and Reynolds, W.C., "A Numerical Investigation of the Compressible Reacting Mixing Layers", *Report No.TF–56*, Stanford University, Department of Mechanical Engineering, Thermosciences Division, Stanford, CA., 1992.

[18] Elliott, G.S. and Samimy, M., Compressibility Effects in Free Shear Layers, AIAA Paper No. 90–0705, 1990.

[19] Dutton, J.C., Burr, R.F., Goebel, S.G., and Messersmith, N.L., Compressibility and Mixing in Turbulent Free Shear Layers, Proc. 12th Symposium on Turbulence, Rolla, MO., 1990.

[20] Clemens, N.T., Paul, P.H., Mungal, M.G., and Hanson, R.K., Scalar Mixing in the Supersonic Shear Layer, AIAA Paper No. 91–1720, 1991.

[21] Hall, J.L., *An Experimental Investigation of Structure, Mixing and Combustion in Compressible Turbulent Shear Layers*. Ph.D. Thesis, California Institute of Technology, Pasadena, CA, 1991.

[22] Givi, P. and Riley, J.J., "Some Current Issues in the Analysis of Reacting Shear Layers: Computational Challenges", *Major Research Topics in Combustion*, (Eds. M.Y. Hussaini, A. Kumar, and R.G. Voigt), Springer–Verlag, New York, NY, 588–650, 1992.

[23] Drummond, J.P. and Givi, P., "Suppression and Enhancement of Mixing in High–Speed Reacting Flow Fields", *Combustion in High-Speed Flows*, (Eds. J. Buckmaster, T.L. Jackson, and A. Kumar), Kluwer Academic Publishers, Boston, MA, 191–229, 1994.

[24] Dimotakis, P.E., "Turbulent Free Shear Layer Mixing and Combustion", *High Speed Propulsion Systems, AIAA Progress Series*, **137**, (Eds. S.N.B. Murthy and E.T. Curran, E. T.), American Institute of Aeronautics and Astronautics, Washington, D.C., ch. 5, 265–340, 1991.

[25] Guirguis, R.H., Grinstein, F.F., Young, T.R., Oran, E.S., Kailasanath, K., and Boris, J.P., Mixing Enhancement in Supersonic Shear Layers, AIAA Paper No. 87–0373, 1987.

[26] Guirguis, R.H., Mixing Enhancement in Supersonic Shear Layers: III. Effect of Convective Mach Number, AIAA Paper No. 88–0701, 1988.

[27] Kumar, A., Bushnell, D.M., and Hussaini, M.Y., "A Mixing Augmentation Technique for Hypervelocity Scramjets", *J. Prop. Power*, **5**, 514–522, 1988.

[28] Drummond, J.P. and Mukunda, H.S., A Numerical Study of Mixing Enhancement in Supersonic Reacting Flow Fields, AIAA Paper No. 88–3260, 1988.

[29] Drummond, J.P., Carpenter, M.H., Riggins, D.W., and Adams, M.S., Mixing Enhancement in a Supersonic Combustor, AIAA Paper No. 89–2794, 1989.

[30] Northam, G.B., Greenberg, I., and Byington, C.S., Evaluation of Parallel Injector Configurations for Supersonic Combustion, AIAA Paper No. 89–2525, 1989.

[31] Marble, F.E., Hendricks, G.J., and Zukoski, E.E., Progress Toward Shock Enhancement of Supersonic Combustion Processes, AIAA Paper No. 87–1880, 1987.

[32] Marble, F.E., Zukoski, E.E., Jacobs, J.W., Hendricks, G.J., and Waitz, I.A., Shock Enhancement of and Control of Hypersonic Mixing and Combustion, AIAA Paper No. 90–1981, 1990.

[33] Carpenter, M.H., Three–Dimensional Computations of Cross–Flow Injection and Combustion in a Supersonic Flow, AIAA Paper No. 89–1870, 1989.

[34] Drummond, J.P., "Supersonic Reacting Internal Flow Fields", *Numerical Approaches to Combustion Modeling, Progress in Astronautics and Aeronautics*, **135**, (Eds. E.S. Oran and J.P. Boris), AIAA Publishing Co., Washington, D.C., ch. 12, 365–420, 1991.